



Cite this: DOI: 10.1039/c8ob02343c

Received 20th September 2018,

Accepted 19th December 2018

DOI: 10.1039/c8ob02343c

rsc.li/obc

ortho-Fluoroazobenzene derivatives as DNA intercalators for photocontrol of DNA and nucleosome binding by visible light†

Benedikt Heinrich,^a Karim Bouazoune,^b Matthias Wojcik,^c Udo Bakowsky^c and Olalla Vázquez^{*a}

We report a high-affinity photoswitchable DNA binder, which displays different nucleosome-binding capacities upon visible-light irradiation. Both photochemical and DNA-recognition properties were examined by UV-Vis, HPLC, CD spectroscopy, NMR, FID assays, EMSA and DLS. Our probe sets the basis for developing new optoeigenetic tools for conditional modulation of nucleosomal DNA accessibility.

Over the last decades, a large number of studies have established that the organization of eukaryotic DNA, by proteins and RNAs, into a nucleoprotein complex referred to as chromatin is key to regulate genome functions.¹ The most abundant chromatin proteins are the histones. These proteins tightly wrap DNA into a “beads-on-a-string”-like structure. Each ‘bead’ is referred to as a nucleosome and comprises a histone octamer around which about 150 base pairs (bp) of DNA are wrapped. On average, nucleosomes are separated by about 50 bp of free (also called “linker”) DNA.² This entails that about 75% of our DNA is wrapped around histones. This nucleosomal organization restricts access to DNA considerably. As a result, nuclear processes such as DNA repair, replication and transcription largely depend on enzymes that can change nucleosomal DNA accessibility.^{3–5}

Hence, the ability to control chromatin compaction and, in turn, DNA accessibility using small molecules may provide us with means to study and, conceivably, control (at least some) genome functions, in physiological as well as disease contexts. So far, the use of small-molecule probes as complementary tools to classic chromatin biochemical approaches has strongly contributed to deciphering epigenetic mechanisms

and strengthened our understanding of genome regulation. However, this approach has mainly been limited to enzyme inhibitors^{6–9} and altering nucleosome accessibility has largely been disregarded. Indeed, while there is just a handful of examples of compounds capable of targeting nucleosomal DNA, to our knowledge, none of these molecules allow spatio-temporal control of nucleosome binding.^{10–15}

Reversible photoresponsive molecules, which have demonstrated their potential in diverse areas (material science,^{16,17} molecular motors^{18–20} photopharmacology,^{21–24} molecular containers,²⁵ *etc.*) represent a very promising chemical alternative to optogenetics.^{26,27} However, the implementation of photoswitchable genome regulators has been very scarce and again only focused on histone-modifying enzymes, so far.^{28–30} Therefore, we designed and synthesized a novel photoswitch, which allows light-driven DNA and nucleosome binding and we studied the consequences of this interaction (Fig. 1a).

The ability of externally controlling DNA-associated processes by switching the state of a photochromic DNA binder has previously been demonstrated.^{31,32} However, such examples are mainly restricted to the use of azo-modified DNA binders, which involve undesirable UV irradiation.^{33–38} There are several strategies to synthesize azobenzene photoswitches that undergo isomerization upon visible-light irradiation.^{39–42} For example, the Hecht group has recently optimized the properties of the classical azobenzenes by introducing σ -electron-withdrawing fluorine atoms in *ortho* position to the azobenzene unit. Such substitution leads to visible-light switches with high photoconversions and very long-lived *cis*-isomers.^{43,44} Furthermore, to our knowledge, photoswitchable DNA binders have never been used in the context of the nucleosome. Consequently, inspired by the natural DNA minor groove binder netropsin (**1**), we synthesized and studied two water-soluble photosensitive pyrrole hybrids that have identical number of *N*-methyl pyrrole rings as netropsin, but incorporate an *ortho*-fluoroazobenzene scaffold between the pyrrole backbone and also vary in terms of their net charge at physio-

^aFachbereich Chemie, Philipps-Universität Marburg, Hans-Meerwein-Straße 4, 35043 Marburg, Germany. E-mail: olalla.vazquez@staff.uni-marburg.de

^bInstitut für Molekularbiologie und Tumorforschung, Philipps-Universität Marburg, Hans-Meerwein-Straße 2, 35043 Marburg, Germany

^cInstitut für Pharmazeutische Technologie & Biopharmazie, Philipps-Universität Marburg, Robert-Koch-Straße 4, 35037 Marburg, Germany

† Electronic supplementary information (ESI) available. See DOI: 10.1039/c8ob02343c

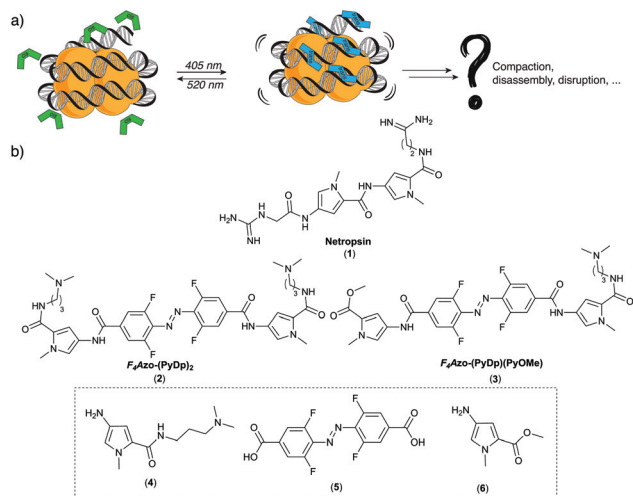


Fig. 1 (a) Outline of the photocontrollable nucleosome targeting approach based on visible-light photoswitchable DNA binders. (b) Structure of the studied molecules, highlighting the key synthetic building blocks.

logical conditions: $F_4\text{Azo}-(\text{PyDp})_2$ (2) and $F_4\text{Azo}-(\text{PyDp})(\text{PyOMe})$ (3) (Fig. 1b).

The synthesis of $F_4\text{Azo}-(\text{PyDp})_2$ (2) and $F_4\text{Azo}-(\text{PyDp})(\text{PyOMe})$ (3) was straightforward through one-pot condensation between the previously reported building blocks: 4,⁴⁵ 5,^{43,44} and 6.⁴⁶ (Fig. 1 & Schemes S1–S4†). Once synthesized, their photochemical behaviour was investigated in detail. Thus, the *ortho*-fluoroazobenzene building block 5 alone and also in presence of the pyrrole moieties showed the expected absorption bands: intense band at $\lambda_{\text{max}} = 319$ nm assigned to the $\pi \rightarrow \pi^*$ transition together with a weaker one due to a $n \rightarrow \pi^*$ and significant intensity decrease of the $\pi \rightarrow \pi^*$ band with a slight increase of the $n \rightarrow \pi^*$ one under 405 nm and 520 nm irradiation, respectively (Fig. S21b†). Nevertheless, the direct insertion of the azophenyl derivative into the pyrrole backbone affected the parental spectra, as observed for related compounds.⁴⁷ Irradiation of $F_4\text{Azo}-(\text{PyDp})_2$ (2) entails fast spectroscopic changes.⁴⁸ Thus, upon irradiation with 520 nm there is a clear intensity decrease between 287 nm and 500 nm, the λ_{max} is slightly shifted to 278 nm and a new partly overlapping band at $\lambda_{\text{max}} = 420$ nm can be detected (Fig. 2a). The photostationary state is reached after just 2 minutes of irradiation. We also demonstrated the reversibility of the photoisomerization for up to 16 cycles without any significant photobleaching (Fig. 2b).

We next determined the isomer ratios at the photostationary state as well as the lifetime of the isomers by integrating the peak area of the HPLC chromatograms at the isobestic point (287 nm). As expected, the *trans*-isomer was the thermodynamically stable species (*trans/cis* ratio 92 : 8; Fig. S23a†). Importantly, the thermal relaxation of the *cis*-isomer was slow (*cis/trans* ratio 77 : 23, after 9 hours stored in the dark, Fig. 3), which enabled both DNA and nucleosome binding experiments.

Unfortunately, $F_4\text{Azo}-(\text{PyDp})(\text{PyOMe})$ (3) did not show any major change neither by UV-Vis spectroscopy nor HPLC

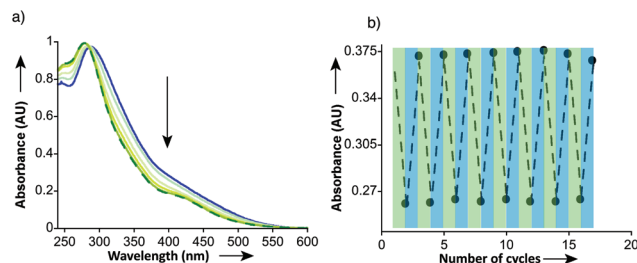


Fig. 2 (a) UV-Vis spectra of a 20 μM solution of $F_4\text{Azo}-(\text{PyDp})_2$ (2) in 10 mM Tris buffer pH 7.6, 50 mM KCl and DMSO (98 : 2), initially at the thermodynamic state (blue) and after successive irradiation intervals at 520 nm (green). (b) Reversible photochromism upon alternating irradiation at 520 nm (green) and 405 nm (blue) measured at 335 nm. Represented data are calculated from three independent experiments.

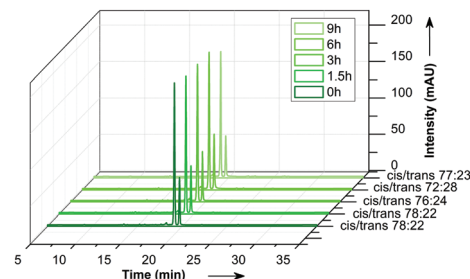


Fig. 3 Evaluation of the *cis*-isomer stability of $F_4\text{Azo}-(\text{PyDp})_2$ (2) in 10 mM Tris buffer pH 7.4, 10 mM NaCl and DMSO (95 : 5) by HPLC after initial irradiation at 520 nm for 2 min (time 0 h). Samples were stored in total darkness. HPLC chromatograms were recorded after the listed times. Represented data are a set, which is representative of the measurements from three independent experiments.

(Fig. S20 & S23b†). This forced us to use $^1\text{H-NMR}$ analysis for further investigations (Fig. 4). Thus, the *trans/cis* ratios were calculated by the integration of the aromatic proton signals (6.8 ppm–8.1 ppm). Gratifyingly, in the case of $F_4\text{Azo}-(\text{PyDp})_2$ (2) we corroborated the same ratio as the one obtained by HPLC (*trans/cis* ratio 93 : 7 and 30 : 70 for the *trans*- and *cis*-state, respectively). In addition, $^1\text{H-NMR}$ studies revealed that, indeed, the photochemical behaviour of $F_4\text{Azo}-(\text{PyDp})(\text{PyOMe})$ (3) is analogous to $F_4\text{Azo}-(\text{PyDp})_2$ (2) (*trans/cis* ratio 97 : 3 and 27 : 73 for the *trans*- and the *cis*-state, respectively).

Once the photoisomerization was fully characterized, we explored whether the two compounds are able to interact with DNA and whether their isomers displayed any differences in DNA-binding affinity. Thermal melting experiments are the most common methodology used for the evaluation of DNA interactions; however, we observed decomposition at high temperatures (Fig. S36†). Consequently, we performed a fluorescent intercalator displacement (FID) assay⁴⁹ compatible with the isomerization. We also compared our results with the minor groove binder netropsin (1). Thiazole orange (TO) was chosen as intercalator since its excitation and emission hardly affect the *trans/cis* isomerization (Fig. S34†). This experiment relies on a decrease of fluorescence due to the displacement of

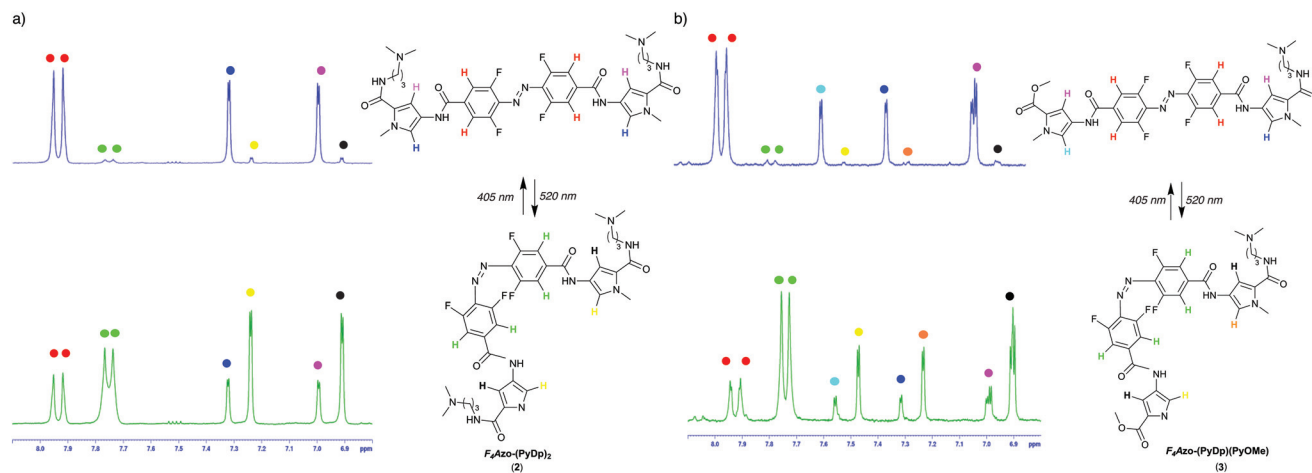


Fig. 4 Selected aromatic region of the ^1H -NMR spectra (300 MHz) of a 4 mM solution of (a) $F_4\text{Azo}-(\text{PyDp})_2$ (**2**) and (b) $F_4\text{Azo}-(\text{PyDp})(\text{PyOMe})$ (**3**) in $\text{DMSO}-d_6$ after irradiation to the *trans*- (top) and *cis*-isomer (bottom). Aromatic protons are marked in colours in the spectra and molecules.

DNA-bound TO by the competitive binder. Therefore, we first determined the apparent binding constant of TO in presence of a hairpin oligonucleotide, which contains the sequence *ATTA* ($\text{dsDNA}_{\text{hAT}}$) with the HypSpec software. Subsequently we simulated the species distribution for the obtained binding constant ($K_D = 59.8 \pm 13.1$ nM) by using the HySS software. The affinity of TO to $\text{dsDNA}_{\text{hAT}}$ enabled FID experiments at low μM range with more than 95% of TO-DNA complex in our experimental conditions (Table S4[†]), which assures the reliability of the assay. Typical fluorescence quenchers such as DABCYL or BHQ-1 are provided with the diazenyl functional group ($\text{R}-\text{N}=\text{N}-\text{R}'$), therefore we initially performed control competition assays in presence of increasing amounts of **5** to rule out artefacts due to quenching effects (Fig. S38[†]). As showed in Fig. 5, both $F_4\text{Azo}-(\text{PyDp})_2$ (**2**) and $F_4\text{Azo}-(\text{PyDp})$

(**PyOMe**) (**3**) were able to efficiently replace the bound TO from the DNA. The obtained data suggested binding modes beyond the 1 : 1 stoichiometry. For the mathematical analysis of the FID assays, the experimental data were fitted globally (all wavelengths simultaneously) with HypSpec. These experimental data fitted the model adequately (Fig. S33[†]).

The analysis of the apparent dissociation constants indicated that both photoswitchable compounds have high DNA-binding affinity in the nM range (Table 1). Importantly, for both azobenzene derivatives (**2** and **3**), the binding capacity of their isomers is different. This demonstrates a conformation-dependent binding mode. In each pair, the *trans*-isomer is always the best binder, which is in agreement with other previous examples of azobenzene derivatives.^{33–38} Furthermore, upon addition of the netropsin (**1**) control, the emission intensity of DNA-bound TO also decreased significantly. The faster saturation of the netropsin (**1**) in comparison with our photo-switchable binders, together with the fact that its binding curve does not appear to follow a standard isotherm may be indicative of different binding modes. It was expected that netropsin (**1**), as a minor groove binder, could not fully displace the intercalator TO and reach saturation.⁵⁰ The binding curve of netropsin (**1**) with a hairpin oligonucleotide containing the sequence *GGCCC* ($\text{dsDNA}_{\text{hGC}}$) displayed the standard

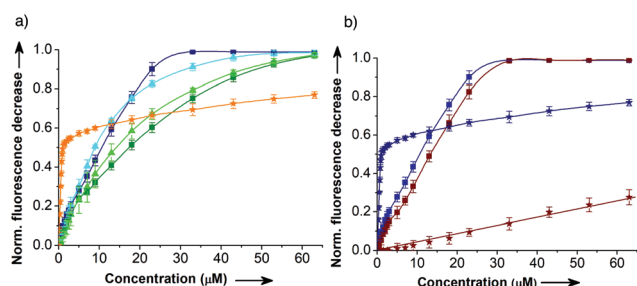


Fig. 5 (a) Competitive displacement analysis of a 6 μM TO solution in 20 mM NaH_2PO_4 pH 7.4, 100 mM NaCl and 1 μM of $\text{dsDNA}_{\text{hAT}}$ with: netropsin (**1**, orange stars); $F_4\text{Azo}-(\text{PyDp})_2$ isomers (*trans*-**2** dark blue squares; *cis*-**2** dark green squares) and $F_4\text{Azo}-(\text{PyDp})(\text{PyOMe})$ (*trans*-**3** light blue triangles; *cis*-**3** light green triangles); (b) sequence-selectivity analysis of netropsin (**1**, stars) *trans*- $F_4\text{Azo}-(\text{PyDp})_2$ (*trans*-**2**, squares) in presence 6 μM TO solution in 20 mM NaH_2PO_4 pH 7.4, 100 mM NaCl and 1 μM of $\text{dsDNA}_{\text{hAT}}$ (blue) or $\text{dsDNA}_{\text{hGC}}$ (brown). Represented data and standard deviations are mean values calculated from three independent experiments. Data points were fitted with HypSpec, using multi-variant factor analysis to obtain globally optimized parameters. Lines are “eye-guides” for assistance in visualizing the binding curves.

Table 1 Binding affinities derived from FID experiments with selected hairpin oligonucleotide (dsDNA_{h})

Compound	dsDNA_{h} site	K_D (nM)
Netropsin (1)	<i>ATTA</i>	10 ± 1
Netropsin (1)	<i>GGCCC</i>	n.c.
<i>cis</i> - $F_4\text{Azo}-(\text{PyDp})(\text{PyOMe})$ (<i>cis</i> - 3)	<i>ATTA</i>	82 ± 6
<i>trans</i> - $F_4\text{Azo}-(\text{PyDp})(\text{PyOMe})$ (<i>trans</i> - 3)	<i>ATTA</i>	54 ± 3
<i>cis</i> - $F_4\text{Azo}-(\text{PyDp})_2$ (<i>cis</i> - 2)	<i>ATTA</i>	108 ± 14
<i>trans</i> - $F_4\text{Azo}-(\text{PyDp})_2$ (<i>trans</i> - 2)	<i>ATTA</i>	60 ± 1
<i>trans</i> - $F_4\text{Azo}-(\text{PyDp})_2$ (<i>trans</i> - 2)	<i>GGCCC</i>	13 ± 1

n.c. represents not calculated.

isotherm for non-specific interaction *i.e.* proportional to the concentration of added ligand (Fig. 5b).

To get additional insight into its binding mode, we performed exemplarily selectivity experiments with $F_4\text{Azo}-(\text{PyDp})_2$ (2) and the additional hairpin $\text{dsDNA}_{\text{hGC}}$ (Fig. 5b) as well as circular dichroism (CD) experiments (Fig. 6).

Regarding selectivity, $F_4\text{Azo}-(\text{PyDp})_2$ (2) showed a slight preference for $\text{dsDNA}_{\text{hGC}}$. Of note, all the obtained binding constants were derived from indirect assessments, based on the TO affinity to the corresponding dsDNA and its loss of fluorescence when it is displaced by a new binder. Therefore, the technique is limited to compounds with binding affinities in the same range. In addition, ligand-induced condensation or interference with the fluorescence could not be discriminated from the actual fluorescence loss due to displacement, which may explain non-standard isotherms. Consequently, these values are, strictly speaking, estimations. Despite these inherent drawbacks, the FID assay is a straightforward method for the comparative characterization of DNA-recognition by the azobenzene derivatives on the one hand, and on the other hand, by netropsin (and compounds with similar binding modes).

The CD experiments of $F_4\text{Azo}-(\text{PyDp})_2$ (2) with the double-stranded *calif thymus* DNA (dsDNA_{CT}) confirmed a non-covalent interaction beyond the external non-specific electrostatic association with the DNA phosphates. Therefore, the observed interaction differs from the cationic polyamines such as spermine and spermidine.⁵¹ The CD spectra of the dsDNA_{CT} alone showed the characteristic bands of the canonical B-DNA conformation (Fig. 6, grey line): a positive band at 275 nm and a negative one at 245 nm of similar intensity.⁵² $F_4\text{Azo}-(\text{PyDp})_2$ (2) is achiral and, hence, optically inactive (Fig. 6, black line). However, when increasing amounts of $F_4\text{Azo}-(\text{PyDp})_2$ (2) were added to the dsDNA_{CT} , induced circular dichroic (ICD) signals were detected, as expected from DNA binders.

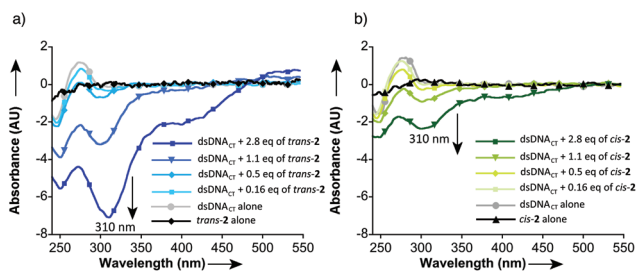


Fig. 6 CD spectra of a 50 μM solution of dsDNA_{CT} in 20 mM NaH_2PO_4 pH 7.4, 100 mM NaCl with increasing amounts of the $F_4\text{Azo}-(\text{PyDp})_2$ isomers: (a) *trans*-2, blue; (b) *cis*-2, green. $F_4\text{Azo}-(\text{PyDp})_2$ amounts: 0 eq. (grey circles); 0.16 eq. (light squares); 0.5 eq. (diamonds); 1.1 eq. (triangles) and 2.8 eq. (dark squares). Black line represents the CD spectra of a 142 μM (equivalent to 2.8 eq. in the titration) solution of $F_4\text{Azo}-(\text{PyDp})_2$ isomers under the same conditions: (a) *trans*-2 (diamonds); (b) *cis*-2 (triangles). Represented data are mean values calculated from two independent experiments; buffer subtracted; eq. means equivalents: mol of compound 2 per mol of dsDNA_{CT} .

Intriguingly, the addition of $F_4\text{Azo}-(\text{PyDp})_2$ (2) induced a remarkable dose-dependent increase in magnitude of the signal in the region of 240–480 nm with a clear negative peak at 310 nm. Importantly, the two isomers *cis*-2 and *trans*-2 behaved differently in the CD experiments under the same conditions. In particular, the ICD signals are more pronounced with *trans*-2 than with *cis*-2, which is concurrent with our previous FID experiments (as described above).

To understand the observed CD signature, we performed UV-Vis titrations (Fig. 7). We observed that the addition of $F_4\text{Azo}-(\text{PyDp})_2$ (2) promoted a red shift of the absorbance maximum of the dsDNA_{CT} and a new partly overlapped band at 420 nm, as in the CD spectra. However, the CD band at 310 nm was not clearly detected in our UV-Vis measurements. Other azo-modified polyamines displayed CD signals at ~ 310 nm in presence of DNA but, to our knowledge, always with positive ellipticity.^{34,53} However, it has been reported that strong insertion of intercalators into the DNA causes a red-shifted band with high negative CD signals between 240 nm and 340 nm,⁵⁴ which is consistent with our observations.

All together our results have shown that $F_4\text{Azo}-(\text{PyDp})_2$ (2) is a photoswitchable molecule capable of interacting with the DNA through a conformation-dependent binding mode.

Finally, we explored the possibility of using $F_4\text{Azo}-(\text{PyDp})_2$ (2) as a controllable nucleosome binder using visible light. For this endeavour, we first reconstituted nucleosome core particles (NCP) using chicken erythrocyte histones⁵⁵ and the Widom 601 DNA, which forms a stably positioned nucleosome.⁵⁶ We next used native gel electrophoretic mobility shift assays (EMSA) to analyse nucleosome reconstitution efficiency. We also used EMSA to assess nucleosome integrity after incubating nucleosomes with increasing amounts of either netropsin (1) or $F_4\text{Azo}-(\text{PyDp})_2$ (2) for three hours. As shown in Fig. 8, low concentrations of the minor groove binder netropsin (up to 4 eq.) do not affect the nucleosome integrity. In the presence of high netropsin concentrations, the bands became very diffuse and consequently barely detectable. This phenomenon may be due to the formation of many different species through unspecific electrostatic interactions^{57,58} and/or aggre-

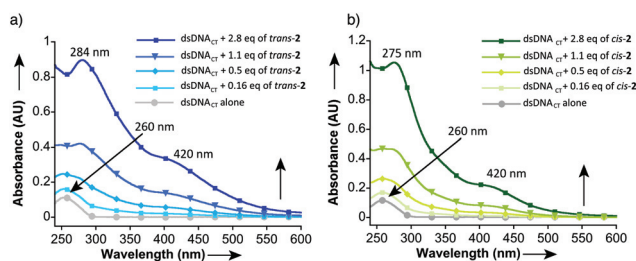


Fig. 7 UV-Vis spectra of a 12.5 μM solution of dsDNA_{CT} in 20 mM NaH_2PO_4 pH 7.4, 100 mM NaCl with increasing amounts of the $F_4\text{Azo}-(\text{PyDp})_2$ isomers: (a) *trans*-2, blue; (b) *cis*-2, green. $F_4\text{Azo}-(\text{PyDp})_2$ amounts: 0 eq. (grey circles); 0.16 eq. (light squares); 0.5 eq. (diamonds); 1.1 eq. (triangles) and 2.8 eq. (dark squares). Represented data are calculated from three independent experiments; buffer was subtracted; eq. means equivalents: mol of compound 2 per mol of dsDNA_{CT} .

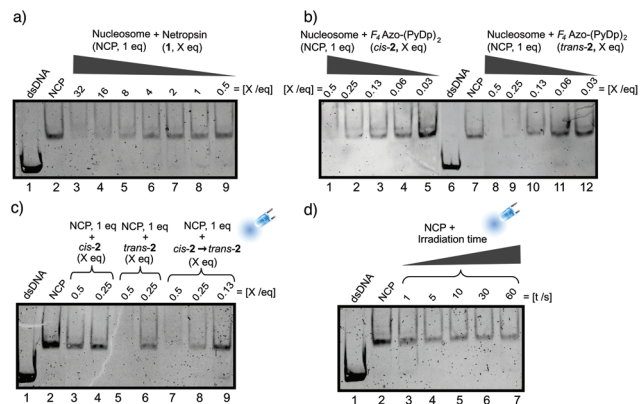


Fig. 8 Evaluation of the interaction of DNA binders with Widom 601 nucleosome core particle (NCP). All experiments were performed with 300 nM NCP and 55 nM dsDNA as control in 10 mM Tris buffer pH 8, 1 mM EDTA, 50 mM NaCl and DMSO (90 : 10) and analyzed by ethidium bromide staining, after electrophoresis: (a) netropsin interaction: lane 1: dsDNA; lanes 2–9: NCP + [netropsin] = 0, 32, 16, 8, 4, 2, 1, 0.5 eq.; (b) $F_4\text{Azo}-(\text{PyDp})_2$ (**2**) interaction: lane 7: NCP; lane 6: dsDNA; lane 1–5: NCP + [*cis-2*] = 0.5, 0.25, 0.13, 0.06, 0.03 eq.; lane 8–12: NCP + [*trans-2*] = 0.5, 0.25, 0.13, 0.06, 0.03 eq. DMSO stocks of $F_4\text{Azo}-(\text{PyDp})_2$ (**2**) were irradiated before EMSA; (c) $F_4\text{Azo}-(\text{PyDp})_2$ (**2**) interaction with *in situ* irradiation: lane 1: dsDNA; lane 2: NCP; lane 3–4: control with previous irradiation of NCP + [*cis-2*] = 0.5, 0.25 eq.; lane 5–6: control with previous irradiation of NCP + [*trans-2*] = 0.5, 0.25; lane 7–9 *in situ* irradiation at 405 nm for 10 s of NCP + [*cis-2*] = 0.5, 0.25, 0.13 eq.; (d) effect of irradiation at 405 nm on NCP: lane 1: dsDNA; lane 2: NCP; lane 3–7: NCP after 1 s, 5 s, 10 s, 30 s, 60 s irradiation. Eq. means equivalents: mol of compound per mol of base pair; NCP means nucleosome core particle.

gates, which may be too big to enter the gel. Interestingly, the binding of our molecule $F_4\text{Azo}-(\text{PyDp})_2$ (**2**) apparently triggered this effect at lower concentrations than netropsin, despite having the same net charge (Fig. 8a & b). Importantly, there was a noticeable difference between isomers. In particular, the intensity of the nucleosome band abruptly ceased to be detectable in the presence of 0.5 eq. of the *trans-2*, while at the same concentration, the *cis-2* failed to fully alter the nucleosome band. Furthermore, the fact that we circumvented the use of strong UV light, for the isomerization, facilitated the *in situ* application. Thus, the same procedure was repeated but now performing the irradiation *in situ*: after incubating the *cis-2* for 1 h with the nucleosome, the samples were irradiated at 405 nm for 10 s, in a single isomerization cycle. As a control, we also included both isomers irradiated prior to the nucleosome incubation. Gratifyingly, we observed that the *in situ* formed *trans-2* showed a higher impact than the parental *cis-2*. Of note, no irradiation effect on the nucleosome was detectable (Fig. 8d).

To complement the EMSA studies and gain preliminary insights into the effect of $F_4\text{Azo}-(\text{PyDp})_2$ (**2**) on the NCPs, we performed dynamic light scattering (DLS) measurements. Nucleosomes are colloidal particles of 11 nm wide,⁵⁹ and alterations in their hydrodynamic size can assist in the characterization of the interaction with small molecules. In this ana-

lysis, we used NCP at 2 μM concentration, employing plasmids containing multiple repeats of the Widom 601 sequence for large-scale DNA preparation.⁶⁰ As shown in Fig. 9, the particle size of the NCP is consistent with previous reports.^{61,62} Increasing amounts of $F_4\text{Azo}-(\text{PyDp})_2$ (**2**) clearly change the size distribution resulting in larger particles than the canonical NCP (Fig. 9a). This effect was reproducible and, interestingly, changes were already detectable from the first $F_4\text{Azo}-(\text{PyDp})_2$ addition (0.06 eq.), although no alterations in the EMSA bands were observable under the same conditions at this concentration (Fig. S46a†). This was also contrary to the case of netropsin, where low concentrations did not affect the size of the particle (Fig. S42 & S46d†). Therefore, as expected, the insertion of $F_4\text{Azo}-(\text{PyDp})_2$ (**2**) caused higher structural distortion than for the minor groove binder **1**. To study the possibility that such distortion leads to aggregation

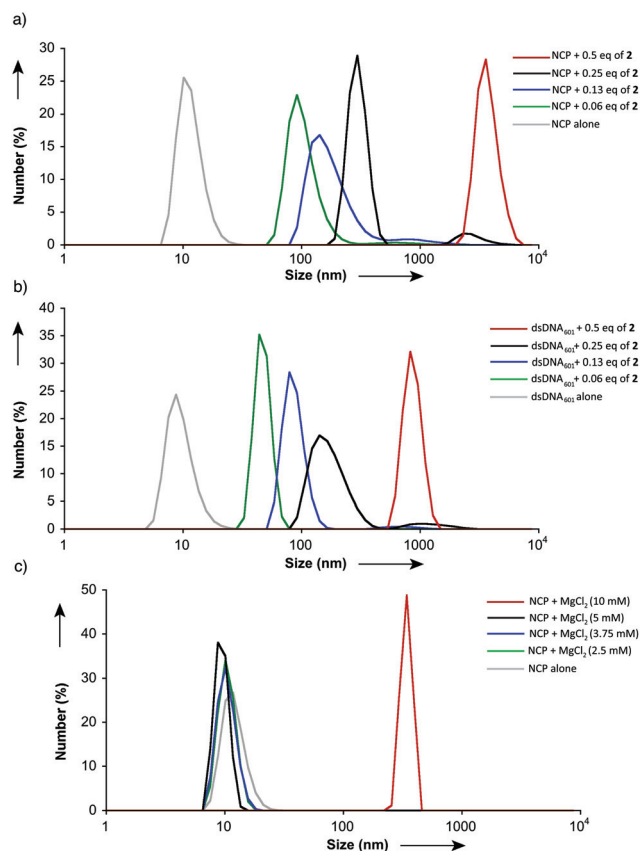


Fig. 9 Effect of $F_4\text{Azo}-(\text{PyDp})_2$ on: (a) nucleosome (NCP); (b) dsDNA₆₀₁ at 2 μM concentration in 10 mM Tris 1 mM EDTA pH 8.0 and 50 mM NaCl monitored by dynamic light scattering (DLS). $F_4\text{Azo}-(\text{PyDp})_2$ (**2**) amounts: 0 eq. (grey); 0.06 eq. (green); 0.13 eq. (blue); 0.25 eq. (black) and 0.5 eq. (red); (c) effect of MgCl₂ on NCP at 2 μM concentration in 3.5 mM Tris 0.35 mM EDTA pH 8.0 monitored by DLS. MgCl₂ concentrations: 0 mM (grey); 2.5 mM (green); 3.75 mM (blue); 5 mM (black); 10 mM (red). Intensity statistics of 10 measurements. Represented data are a representative one of two measurements from independent experiments; eq. means equivalents (mol of compound per mol of base pair) Represented data are a set, which is representative of the measurements from two independent experiments.

via nucleosome disassembly, we performed control experiments with the analogue set-up but using the dsDNA employed for the nucleosome assembly (dsDNA₆₀₁) instead of the whole NCP, as well as, the precipitated NCP in presence of magnesium chloride; and histone octamer alone. However, the latter protein complex did not display any DLS signal under these conditions. 10 mM of magnesium chloride promoted the precipitation of the NCP (Fig. S43 & S46c†) and the appearance of single peak of higher size than the NCP alone but smaller than the one obtained with highest concentrations of *F*₄Azo-(PyDp)₂ (2) (342 nm versus 3580 nm, respectively). Interestingly, the incubation of dsDNA₆₀₁ in presence of *F*₄Azo-(PyDp)₂ (2) (Fig. 9B) displayed DNA-higher order structures, as reported with other cationic molecules^{63–65} such as polyamines, surfactants, etc. Qualitatively, the distribution of the peaks obtained from this titration were similar to the one observed in the presence of NCP (Fig. 9a). Therefore, these DLS data suggest that, first, the *F*₄Azo-(PyDp)₂ (2) intercalates into the nucleosomal DNA inducing distortions, which lead to the formation of high size aggregates. These observations are consistent with the hypothesis that nucleosome distortion subsequently leads to disruption. Future experiments will be required to fully characterize these alterations and their kinetics.

In summary, we have designed, synthesized and studied a novel photoswitchable *ortho*-fluoroazobenzene DNA binder: *F*₄Azo-(PyDp)₂. We also demonstrated that its DNA interaction depends on the conformation, which, importantly, can be controlled by visible-light. Furthermore, our study establishes the possibility of performing photocontrollable nucleosome binding. To our knowledge this is the first time that nucleosome targeting is externally modulated by visible-light photo-switches. We believe that this approach uncovers the possibility of using photosensitive chemical tools to alter nucleosome-based processes. At this point, it is impossible to predict whether our molecule can preferentially impact specific cell functions. It is more plausible that, if appropriately taken up by cells, the molecule would alter cell functions randomly, since *F*₄Azo-(PyDp)₂ (2) only shows a slight sequence binding preference. Thus, future directions may include the development of sequence-specific nucleosome binders to potentially control cell functions specifically via modulation of DNA transcription and/or repair processes.

Conflicts of interest

There are no conflicts to declare.

Acknowledgements

The authors gratefully acknowledge: Prof. E. Meggers (Phillips-Universität Marburg) for the accessibility to his S1 laboratory; Prof. P. Ballester (ICIQ) for the insight into the use of HypSpec and HySS software; Prof. S. Hecht (Humboldt-Universität zu

Berlin) for the discussions and suggestions regarding the initial isomerization irradiation experiments; Prof. A. Brehm (IMT Marburg) for critical advice and support; Prof. J.-J. Song (Korea Advanced Institute of Science and Technology) for supplying the plasmid pUC-19/16X601; M. Alawak and J. Schäfer (Phillips-Universität Marburg) for initial discussions regarding DLS; N. Frommknecht (Phillips-Universität Marburg) for design assistance and construction of LED lamps; COST action CM1406 (Epigenetic Chemical Biology EPICHEMBO) for support in networking and mutual cooperation. O. V. thanks the SPP1926 for the Young Investigator Award and Fulbright Commission for the Fulbright-Cottrell Award 2016. Finally, this work was financially supported by Fulbright Commission and the DFG programs: SPP1926 'Next Generation Optogenetics', Young Investigator program (grant # GO1011/11-1) and TRR81: 'Chromatin Changes in Differentiation and Malignancies' (TRR81/3, Z04).

Notes and references

- G. Felsenfeld, *Cold Spring Harbor Perspect. Biol.*, 2014, **6**(1), a018200.
- D. E. Schones, K. Cui, S. Cuddapah, T. Y. Roh, A. Barski, Z. Wang, G. Wei and K. Zhao, *Cell*, 2008, **132**(5), 887–898.
- K. Luger, *Chromosome Res.*, 2006, **14**(1), 5–16.
- C. R. Clapier and B. R. Cairns, *Annu. Rev. Biochem.*, 2009, **78**, 273–304.
- C. D. Allis and T. Jenuwein, *Nat. Rev. Genet.*, 2016, **17**(8), 487–500.
- C. D. Allis and T. W. Muir, *ChemBioChem*, 2011, **12**(2), 264–279.
- A. Huston, C. H. Arrowsmith, S. Knapp and M. Schapira, *Nat. Chem. Biol.*, 2015, **11**(8), 542–545.
- J. Shortt, C. J. Ott, R. W. Johnstone and J. E. Bradner, *Nat. Rev. Cancer*, 2017, **17**(4), 160–183.
- P. A. Cole, *Nat. Chem. Biol.*, 2008, **4**(10), 590–597.
- J. D. Trzuppek, J. M. Gottesfeld and D. L. Boger, *Nat. Chem. Biol.*, 2006, **2**(2), 79–82.
- E. Y. Chua, G. E. Davey, C. F. Chin, P. Droge, W. H. Ang and C. A. Davey, *Nucleic Acids Res.*, 2015, **43**(11), 5284–5296.
- R. K. Suto, R. S. Edayathumangalam, C. L. White, C. Melander, J. M. Gottesfeld, P. B. Dervan and K. Luger, *J. Mol. Biol.*, 2003, **326**(2), 371–380.
- R. S. Edayathumangalam, P. Weyermann, J. M. Gottesfeld, P. B. Dervan and K. Luger, *Proc. Natl. Acad. Sci. U. S. A.*, 2004, **101**(18), 6864–6869.
- C. T. McMurray and K. E. van Holde, *Proc. Natl. Acad. Sci. U. S. A.*, 1986, **83**(22), 8472–8476.
- M. E. Nunez, K. T. Noyes and J. K. Barton, *Chem. Biol.*, 2002, **9**(4), 403–415.
- M. M. Russew and S. Hecht, *Adv. Mater.*, 2010, **22**(31), 3348–3360.
- J. Karcher and Z. L. Pianowski, *Chem. – Eur. J.*, 2018, **24**(45), 11605–11610.

- 18 L. A. Huber, K. Hoffmann, S. Thumser, N. Bocher, P. Mayer and H. Dube, *Angew. Chem., Int. Ed.*, 2017, **56**(46), 14536–14539.
- 19 A. S. Lubbe, Q. Liu, S. J. Smith, J. W. de Vries, J. C. M. Kistemaker, A. H. de Vries, I. Faustino, Z. Meng, W. Szymanski, A. Herrmann and B. L. Feringa, *J. Am. Chem. Soc.*, 2018, **140**(15), 5069–5076.
- 20 T. van Leeuwen, A. S. Lubbe, P. Stacko, S. J. Wezenberg and B. L. Feringa, *Nat. Rev. Chem.*, 2017, **1**(12), 96.
- 21 J. Broichhagen, J. A. Frank and D. Trauner, *Acc. Chem. Res.*, 2015, **48**(7), 1947–1960.
- 22 K. Hull, J. Morstein and D. Trauner, *Chem. Rev.*, 2018, **118**(21), 10710–10747.
- 23 M. M. Lerch, M. J. Hansen, G. M. van Dam, W. Szymanski and B. L. Feringa, *Angew. Chem., Int. Ed.*, 2016, **55**(37), 10978–10999.
- 24 W. A. Velema, W. Szymanski and B. L. Feringa, *J. Am. Chem. Soc.*, 2014, **136**(6), 2178–2191.
- 25 A. Diaz-Moscoso and P. Ballester, *Chem. Commun.*, 2017, **53**(34), 4635–4652.
- 26 M. Banghart, K. Borges, E. Isacoff, D. Trauner and R. H. Kramer, *Nat. Neurosci.*, 2004, **7**(12), 1381–1386.
- 27 L. Fenno, O. Yizhar and K. Deisseroth, *Annu. Rev. Neurosci.*, 2011, **34**, 389–412.
- 28 L. Albert, J. Xu, R. W. Wan, V. Srinivasan, Y. L. Dou and O. Vazquez, *Chem. Sci.*, 2017, **8**(6), 4612–4618.
- 29 S. A. Reis, B. Ghosh, J. A. Hendricks, D. M. Szantai-Kis, L. Tork, K. N. Ross, J. Lamb, W. Read-Button, B. Zheng, H. Wang, C. Salthouse, S. J. Haggarty and R. Mazitschek, *Nat. Chem. Biol.*, 2016, **12**(5), 317–323.
- 30 W. Szymanski, M. E. Ourailidou, W. A. Velema, F. J. Dekker and B. L. Feringa, *Chemistry*, 2015, **21**(46), 16517–16524.
- 31 A. S. Lubbe, W. Szymanski and B. L. Feringa, *Chem. Soc. Rev.*, 2017, **46**(4), 1052–1079.
- 32 E. Pazos, J. Mosquera, M. E. Vazquez and J. L. Mascarenas, *ChemBioChem*, 2011, **12**(13), 1958–1973.
- 33 A. Bergen, S. Rudiuk, M. Morel, T. Le Saux, H. Ihmels and D. Baigl, *Nano Lett.*, 2016, **16**(1), 773–780.
- 34 M. Deiana, Z. Pokladek, J. Olesiak-Banska, P. Mlynarz, M. Samoc and K. Matczyszyn, *Sci. Rep.*, 2016, **6**, 28605–28611.
- 35 S. Ghosh, D. Usharani, A. Paul, S. De, E. D. Jemmis and S. Bhattacharya, *Bioconjugate Chem.*, 2008, **19**(12), 2332–2345.
- 36 C. Dohno, S. N. Uno and K. Nakatani, *J. Am. Chem. Soc.*, 2007, **129**(39), 11898–11899.
- 37 T. Stafforst and D. Hilvert, *Angew. Chem., Int. Ed.*, 2010, **49**(51), 9998–10001.
- 38 T. Goldau, K. Murayama, C. Brieke, S. Steinwand, P. Mondal, M. Biswas, I. Burghardt, J. Wachtveitl, H. Asanuma and A. Heckel, *Chem. – Eur. J.*, 2015, **21**(7), 2845–2854.
- 39 J. Garcia-Amoros and D. Velasco, *Beilstein J. Org. Chem.*, 2012, **8**, 1003–1017.
- 40 H. M. Bandara and S. C. Burdette, *Chem. Soc. Rev.*, 2012, **41**(5), 1809–1825.
- 41 M. X. Dong, A. Babalhavaeji, S. Samanta, A. A. Beharry and G. A. Woolley, *Acc. Chem. Res.*, 2015, **48**(10), 2662–2670.
- 42 D. Bleger and S. Hecht, *Angew. Chem., Int. Ed.*, 2015, **54**(39), 11338–11349.
- 43 D. Bleger, J. Schwarz, A. M. Brouwer and S. Hecht, *J. Am. Chem. Soc.*, 2012, **134**(51), 20597–20600.
- 44 C. Knie, M. Utecht, F. Zhao, H. Kulla, S. Kovalenko, A. M. Brouwer, P. Saalfrank, S. Hecht and D. Bleger, *Chemistry*, 2014, **20**(50), 16492–16501.
- 45 C. Hotzel, A. Marotto and U. Pindur, *Eur. J. Med. Chem.*, 2002, **37**(5), 367–378.
- 46 N. R. Wurtz, J. M. Turner, E. E. Baird and P. B. Dervan, *Org. Lett.*, 2001, **3**(8), 1201–1203.
- 47 R. Sekiya, A. Diaz-Moscoso and P. Ballester, *Chemistry*, 2018, **24**(9), 2182–2191.
- 48 C. W. Ong, Y. T. Yang, M. C. Liu, K. R. Fox, P. H. Liu and H. W. Tung, *Org. Biomol. Chem.*, 2012, **10**(5), 1040–1046.
- 49 D. L. Boger, B. E. Fink, S. R. Brunette, W. C. Tse and M. P. Hedrick, *J. Am. Chem. Soc.*, 2001, **123**(25), 5878–5891.
- 50 Y. W. Ham, W. C. Tse and D. L. Boger, *Bioorg. Med. Chem. Lett.*, 2003, **13**(21), 3805–3807.
- 51 H. Deng, V. A. Bloomfield, J. M. Benevides and G. J. Thomas Jr., *Nucleic Acids Res.*, 2000, **28**(17), 3379–3385.
- 52 J. Kypr, I. Kejnovska, D. Renciuik and M. Vorlickova, *Nucleic Acids Res.*, 2009, **37**(6), 1713–1725.
- 53 M. Deiana, Z. Pokladek, K. Matczyszyn, P. Mlynarz, M. Buckle and M. Samoc, *J. Mater. Chem. B*, 2017, **5**(5), 1028–1038.
- 54 F. Livolant and M. F. Maestre, *Biochemistry*, 1988, **27**(8), 3056–3068.
- 55 C. L. Peterson and J. C. Hansen, *CSH Protoc*, 2008, **3**(12), 1–8.
- 56 R. D. Makde, J. R. England, H. P. Yennawar and S. Tan, *Nature*, 2010, **467**(7315), 562–566.
- 57 E. K. Liebler and U. Diederichsen, *Org. Lett.*, 2004, **6**(17), 2893–2896.
- 58 O. Vazquez, J. B. Blanco-Canosa, M. E. Vazquez, J. Martinez-Costas, L. Castedo and J. L. Mascarenas, *ChemBioChem*, 2008, **9**(17), 2822–28229.
- 59 A. Bertin, S. Mangenot, M. Renouard, D. Durand and F. Livolant, *Biophys. J.*, 2007, **93**(10), 3652–3663.
- 60 P. N. Dyer, R. S. Edayathumangalam, C. L. White, Y. Bao, S. Chakravarthy, U. M. Muthurajan and K. Luger, *Methods Enzymol.*, 2004, **375**, 23–44.
- 61 A. Banerjee, P. Majumder, S. Sanyal, J. Singh, K. Jana, C. Das and D. Dasgupta, *FEBS Open Bio*, 2014, **4**, 251–259.
- 62 Y. Arimura, H. Kimura, T. Oda, K. Sato, A. Osakabe, H. Tachiwana, Y. Sato, Y. Kinugasa, T. Ikura, M. Sugiyama, M. Sato and H. Kurumizaka, *Sci. Rep.*, 2013, **3**, 3510.
- 63 D. Baigl and K. Yoshikawa, *Biophys. J.*, 2005, **88**(5), 3486–3493.
- 64 S. Rudiuk, S. Franceschi-Messant, N. Chouini-Lalanne, E. Perez and I. Rico-Lattes, *Langmuir*, 2008, **24**(16), 8452–8457.
- 65 A. Venancio-Marques, A. Bergen, C. Rossi-Gendron, S. Rudiuk and D. Baigl, *ACS Nano*, 2014, **8**(4), 3654–3663.